Models of Indoor Radio Propagation: Theory and Practice

Master's Thesis submitted to the
Faculty of Informatics of the *Università della Svizzera Italiana*
in partial fulfillment of the requirements for the degree of
Master of Science in Embedded Systems Design

presented by
Jasmina Manojlovic

under the supervision of
Prof. Miroslaw Malek
co-supervised by
Dr. Anna Förster

January 2014

I certify that except where due acknowledgement has been given, the work presented in this thesis is that of the author alone; the work has not been submitted previously, in whole or in part, to qualify for any other academic award; and the content of the thesis is the result of work which has been carried out since the official commencement date of the approved research program.

Jasmina Manojlovic
Lugano, pending January 2014

To my beloved parents and sister

It always seems impossible until it is done.

Nelson Mandela

Abstract

Before implementing designs and confirming planning of wireless communication systems, accurate propagation characteristics of the environment should be known. Indoor environment poses great challenges for modelling of wireless signal propagation, as the effects of diffraction and scattering from both walls and furniture cause the wireless channel to be time-varying, with significant amount of path loss. The accurate prediction of path loss is a crucial element for link budgeting and coverage estimation.

The 'Improved Empirical Model for Indoor Propagation Prediction' which incorporates the wall attenuation factor and different path loss indexes at the two sides of the break point distance has been implemented on the top of the Radio Irregularity Model and simulated in MATLAB for two different types of walls. The measurements of radio irregularity and signal loss through the walls have been carried out for comparison with simulation results.

By graphically analyzing the experimentally obtained data, it was observed that the convexity of the curves was not in line with the results of simulation, which were initially done using the available empirical model.

Taking into consideration the very important fact that path loss is a function of distance, a fundamental observation brought forth by this work is that the existing model does not take into account a different rate of path loss increase before and after the wall, which can explain the disparity between simulated and measured results. Accounting for the different rates of signal loss from each side of the wall, an enhanced model of wireless signal propagation which factors in the distance of the wall from the transmitter and the new path loss indexes has been proposed. It has been shown that experimentally measured values closely resemble those obtained by simulating the new enhanced model.

Acknowledgements

At the onset let me begin by saying that it takes a special guide to ignite the spark of passion and ever burning motivation in the mind of a student towards a technical goal and I consider myself privileged to have had the opportunity to learn and grow under the tutelage of Dr. Anna Förster during the development of this work. I would like to gratefully and sincerely thank Dr. Förster for her understanding, patience and most importantly friendship during the course of my thesis from inception to completion. Despite her busy schedule, Dr. Förster was always available to clarify my doubts and provide me with direction whenever needed. I consider myself truly fortunate to have had this opportunity to grow my intellectual prowess and sharpen my critical thinking under her watchful supervision.

I would like to express my deep gratitude and respect to Prof. Miroslaw Malek whose advice and insight has been invaluable to me. His attitude, zeal and enthusiasm towards research has inspired me to scale greater heights in future professional life. I would also like to thank Ing. Rami Baddour for his helpful suggestions and support during the course of my thesis.

I would like to express my sincere gratitude to Prof. Mariagiovanna Sami for giving me an opportunity to pursue my Masters at ALaRI. I would also like to thank and extend my gratitude to Umberto Bondi, Daniela Dimitrova, Janine Caggiano and the entire staff at ALaRI and USI for their generous help and support throughout my studies.

Finally I take this opportunity to express deep gratitude towards my parents and sister whose selfless love, affection and dedication, nourished and empowered me to accomplish all goals in life. Their support, encouragement, quiet patience and unwavering love are undeniably the bedrock upon which my life has been built.

Contents

Figures

Tables

Chapter 1

Introduction

The explosive growth of indoor wireless communications in recent years has made the domain of propagation modeling a subject of intense investigation. Indoor environments pose great challenges for wireless signal propagation, as the transmitted signal often reaches the receiver through multiple walls and floors. The characteristics of propagation must be taken into account while determining the optimum receiving locations and estimating the coverage area. The ability to accurately predict radio-propagation behavior is crucial for system design. It is therefore important to develop effective propagation models, in order to provide design guidelines for indoor wireless communication systems.

A typical indoor radio channel is a time-varying system which demonstrates highly random behavior. It varies greatly with the environment and depends heavily on building layout and structure of the room due to reflection, diffraction and scattering from walls, windows, doors, etc. inside the building. As a consequence, many variables are involved in the process of modeling the indoor wireless channel, which is not a trivial task.

During wireless signal propagation, an interaction between the waves and the environment attenuates the signal level. This causes path loss which finally limits the coverage area. Models that accurately predict the path loss are essential for link budgeting and coverage estimation. The link budget is the fundamental calculation for planning of any Radio Frequency (RF) link between the transmitter and the receiver. The result of the link budget calculations is the maximum allowable path loss PL in RF link wik [b]:

$$PL = P_T + G_T + G_R - P_R - L_T - L_R \quad [dB] \tag{1.1}$$

where:

P_T and P_R are the transmitted and the received power;

G_T and G_R are gains of the transmitting and the receiving antenna;

L_T and L_R are the transmitting and the receiving antenna losses;

All the parameters are in a dB scale.

Essentially, there are two main types of propagation models: empirical and deterministic. The former are based on statistical characterization of the received signal. They are easier to implement, require less computational effort and are less sensitive to the physical surroundings. The latter require vast amount of specific data regarding environment geometry, building layout, position of furniture in rooms, etc. Deterministic models are more accurate but also more computationally intensive. The empirical and deterministic approaches to modeling make very different trade-offs between complexity and accuracy.

The contribution of this work is manifold:

- A thorough comparative analysis of existing empirical models for indoor propagation environment has been performed.
- The performance and prediction capabilities of existing state of the art empirical models have been evaluated via simulation in MATLAB. They were shown to only badly mimic experimental results.
- A new model has been proposed. The newly proposed model credibly corresponds to reality, lowering the total error from over 30% to as little as 7.5%.

Empirical propagation models usually represent a set of equations derived from extensive field measurements. Therefore they are specific to the type of environment and communication system parameters. Current research trend focuses on improving the performance of these models while retaining the straight-forwardness in their implementation. It is very valuable to have the capability of accurately predicting signal path loss required for network coverage analysis without conducting a series of on-site propagation measurements which are very expensive and time consuming.

The rest of this work is organized as follows: Chapter 2- 'State of the Art' gives formal definitions of RF signal path loss, introduces the Power law and provides an overview of relevant propagation models for the indoor environments. The propagation models discussed include the models which address the path loss prediction and the Radio Irregularity Model which consolidates the radio irregularity phenomena occurring in physical reality during wireless signal propagation. In Chapter 3 - 'Problem Statement', the concept of embedding the empirical path loss model into the Radio Irregularity Model is considered with the aim of obtaining realistic and more accurate received signal strength prediction. Second aspect regards the wall attenuation factors and their importance for modeling of indoor environment. Chapter 4 - 'Measurements of Radio Irregularity' describes the process of measuring and computing the Degree of Irregularity, the parameter which is fundamental for modeling procedure. Chapter 5 - 'Wall Attenuation Measurements' outlines the propagation parameters of the empirical model. Based on their analysis, the measurement and simulation scenarios are derived. The measurements of signal attenuation after passing through the wall are presented. Implementation of simulator is explained in detail in Chapter 6 - 'Simulation in MATLAB'. The results of simulation are analyzed and compared to the measurements. Finally, the new empirical model is presented in Chapter 7 'Proposition of a new model'.

Chapter 2

State of the Art

"The mobile radio channel places fundamental limitations on the performance of wireless communication systems."

Theodore S. Rappaport

Radio propagation models serve as a powerful method for predicting the average received signal strength at an arbitrary distance from the transmitter. There are essentially two types of models according to Rappaport [2001]: large-scale models which predict the mean signal strength over large transmitter-receiver (T-R) separation distances, and small-scale models that portray rapid fluctuations of the received signal strength over short distances of a few wavelengths. In this work large-scale indoor propagation models are of interest, as they are used for predicting the local average signal level at the distances much greater than the couple of wavelengths.

Since the local average received signal strength gradually decreases as propagated further from the transmitter, it is necessary to perform the path loss analysis. Path loss normally occurs due to

- The natural propagation of the radio wavefront in free space (theoretically in the shape of a sphere)
- Absorption (or penetration) losses
- Diffraction losses

Before discussing the existing indoor propagation models, the necessary path loss calculation is described in detail.

2.1 Path Loss

2.1.1 Free Space Path Loss

In cases where no obstacles exist between the transmitter and the receiver (e.g. there is a clear line-of-sight), the signal is said to exhibit free space propagation. This propagation is depicted

by Friis free space equation, which is used to calculate the received power P_r:

$$P_r(d) = \frac{P_t G_t G_r \lambda^2}{(4\pi)^2 d^2 L} \tag{2.1}$$

where:

P_t is the transmitted power. Both P_r and P_t are expressed in Watts;

G_t and G_r are the transmitter and receiver antenna gain respectively. They are dimensionless entities;

λ is the signal wavelength in meters;

d is the T-R separation distance in meters;

L is the system loss factor, which is not related to the propagation.

L takes into account antenna loses, filter loses and transmission line attenuation in the communication system. If L=1 no loss in the system hardware is assumed Rappaport [2001].

All radio signals undergo attenuation when propagating through free space - this is referred to as free space path loss. The path loss is a positive quantity measured in dB, defined as the difference between the effective transmitted power and the received power Rappaport [2001]:

$$PL(dB) = 10log\left(\frac{P_t}{P_r}\right) = -10log\left[\frac{G_t G_r \lambda^2}{(4\pi)^2 d^2}\right] \tag{2.2}$$

If the antennas have unity gain (i.e $G_t = G_r = 1$), these constants may be excluded from the previous equation:

$$PL(dB) = 10log\left(\frac{P_t}{P_r}\right) = -10log\left[\frac{\lambda^2}{(4\pi)^2 d^2}\right] \tag{2.3}$$

It is important to note that Friis free space equation (2.1) holds only when the receiver is placed in the far-field of the transmitting antenna. The far-field, or Fraunhofer region, is referred to as the region beyond the far-field distance d_f Rappaport [2001], given by:

$$d_f = \frac{2D^2}{\lambda} \tag{2.4}$$

where D is the largest physical linear dimension of antenna. The receiver is considered to be in the far-field if it satisfies $d_f \gg D$ and $d_f \gg \lambda$. Former also implies the large-scale propagation.

Moreover, one could obviously see that the equation (2.1) does not hold for $d = 0$. Therefore, the reference distance d_0 is introduced in large-scale propagation models as the known received power reference point. Any received power at a given distance $d \geq d_0$ can be related to power received at $_0$, $P_r(d_0)$, as

$$P_r(d) = P_r(d_0)\left(\frac{d_0}{d}\right)^2 \quad \text{when } d \geq d_0 \geq d_f. \tag{2.5}$$

The reference distance has to be chosen to lie within the far-field region, i.e $d_0 > d_f$. It also has to be smaller than any practical distance used in the transmission system. $P_r(d_0)$ will be explained more in detail in the following section.

Due to the large dynamic range of received power levels, it is more convenient to express them in dBm. This could be done by applying the logarithm to (2.5):

$$P_r(d)[dB] = 10\,log\left[\frac{P_r(d_0)}{0.001W}\right] + 20\,log\left(\frac{d_0}{d}\right) \quad \text{when } d \geq d_0 \geq d_f. \tag{2.6}$$

2.1.2 Log-distance Path Loss

Manier time it has been proved both theoretically and experimentally that the average received signal strength decays logarithmically with the distance from the transmitter, raised to the power n. The average large-scale path loss is therefore modeled as the power law:

$$\overline{PL}[dB] = \overline{PL}(d_0) + 10\,n\,log\left(\frac{d}{d_0}\right) \tag{2.7}$$

The bars in the equation stand for the average values. $PL(d_0)$ is called the reference path loss; it represents a free space propagation from the transmitter up to the reference distance d_0. It is easily calculated using equation 2.2 or 2.3 of the Friis' model (or obtained through the field measurements at d_0). Reference distance has to be placed in the transmitting antenna's far-field, so that the near field effects do not influence the received signal. For micro-cellular systems d_0 normally ranges from 1 m up to 100 m, while in large cellular systems 1 km is usually used.

After d_0, the path loss increases exponentially with the distance. This is depicted by the mean path loss exponent n, that indicates the rate at which the path loss increases along the T-R separation distance d. The path loss index strongly depends on the environment. In free space n typically equals 2, but it becomes larger in presence of obstructions.

To summarize, the path loss is considered to be log-normally distributed about the mean power law (2.7).

2.2 Indoor Propagation Models

The indoor radio channel is difficult to model since it varies greatly with the environment. The electromagnetic wave propagation depends heavily on the building structure, room layout and the type of construction materials. The amount of signal attenuation differs significantly depending on whether the doors are open or closed, where the antennas are mounted, etc. Short T-R distances make it difficult to ensure the receiver is in the far-field of the transmitter.

As the properties of an indoor radio channel are particular to a given environment, researchers have focused their efforts on deriving large scale propagation models from empirical data measured within various building types.

2.2.1 Addition of Attenuation Factors to the Log-distance Model

Propagation models in Seidel and Rappaport [1992] make use of site-specific information in order to predict the signal path loss inside buildings. More precisely, the models are developed

so they take into account the effects of walls, office partitions and floors found between the transmitter and the receiver. They are based on the extensive measurements of received signal strength at 914 MHz, which have been carried out inside of a multistory office building. The purpose of this work was to investigate the amount of attenuation introduced by preceding obstacles. This was done by statistically analyzing the obtained measurements, classifying the results according to the physical surroundings and making use of the resulting values in the models.

At first, the average large-scale path loss model (2.7) was used for the path loss prediction at measured locations. Next, the assumption was made that the mean path loss exponent n is "a function of building type, building wing and number of floors between transmitter and receiver" Seidel and Rappaport [1992]. For this reason, the received signal strength measurements were performed by placing the transmitter and the receiver such that the signal traversed multiple obstructions like floors, concrete walls, cloth-covered office partitions and windows. The path loss values were simply obtained by subtracting received signal strengths from the transmitter power ($Path\,Loss = Transmitted\ Power - Received\ Signal\ Strength$).

Since the distribution of measured path loss data is log-normal, the following applies:

$$PL(d)[dB] = \overline{PL}(d)[dB] + X_\sigma[dB] \tag{2.8}$$

The above equation is commonly known as Log-normal Shadowing Model. A log-normally distributed random variable X_σ has zero mean and standard deviation σ in dB. Standard deviation σ can be seen as a quantitative measure of the accuracy of the path loss predicted by the average large-scale path loss model (2.7). Thus, the mean path loss exponent n and standard deviation σ can be computed by means of linear regression and minimum square error. In order to evaluate parameters n and σ as a function of the physical surroundings, the data has been grouped by building wing and the number of floors which signal traversed between the transmitter and receiver. Standard deviation for the entire office building is observed to be 12.8 dB and for the same floor measurements it was 11.2 dB. Further classification into same floor measurements for separated building wings - West and Central Wing, reduces sigma to 8.1 dB and 4.3 dB, respectively.

One could easily foresee that the propagation through multiple floors leads to a severe increase in path loss for a given T-R separation, but a simple d^n model (2.7) does not take into account the number of floors and office partitions that signal is traversing. Therefore, it was further concluded that the mean path loss exponent has to be function of the number of floors present in T-R separation, and (2.7) can be modified to:

$$\overline{PL}(d)[dB] = PL(d_0)[dB] + 10n(multifloor)log\left(\frac{d}{d_0}\right) \tag{2.9}$$

An alternative way to account for the signal attenuation through multiple floors is to introduce a constant floor factor to the path loss prediction model. The Floor Attenuation Factor (FAF) should differ depending on the building type and the number of floors. In this case, the path loss exponent n for the same floor should be used for the particular building type:

$$\overline{PL}(d)[dB] = PL(d_0)[dB] + 10n(same\_floor)log\left(\frac{d}{d_0}\right) + FAF[dB] \tag{2.10}$$

This model is known as Floor Attenuation Factor Path Loss Model. The *FAF* values were computed as an average of the difference between the measured path loss and the mean path loss predicted by (2.7).

Interesting point here is that the average first floor FAF value does not simply sum up as the number of floors gets bigger, but it is rather a nonlinear function of number of floors found between the transmitter and the receiver.

Although the use of both (2.9) and (2.10) results in a reduction of the standard deviation, one last refinement could be done. For the same floor measurements, a distinction between concrete walls and soft partitions could be taken into account. In this case, soft partitions refer to partitions which can be moved and do not span to the ceiling Rappaport [2001]. Therefore, the Floor Attenuation Factor Path Loss Model changes into:

$$\begin{aligned}\overline{PL}(d)[dB] = 20log\left(\frac{4\pi d}{\lambda}\right) + pAF(soft\_partition)[dB] \\ + qAF(concrete\_wall)[dB]\end{aligned} \tag{2.11}$$

where p is the number of soft partitions and q is the number of concrete walls that lie directly between the transmitter and the receiver. Instead of log-distance models with path loss index, here a free space propagation is assumed for all distances (hence the factor 20 log and no reference distance), and the attenuation factors for each concrete wall and soft partition are added to model the attenuation.

An additional set of measurements was run at the same floor of the office building with the walls and partitions obstructing the signal propagation path. The difference is computed between the measured path loss values and the predicted values in case of free space propagation. Assuming all soft partitions produce identical loss and all concrete walls produce identical loss, linear regression and minimum mean square error can be used to find the best fit for the attenuation factors. When these attenuation factor values are put back into (2.11), the standard deviation of the difference between the measured and predicted path loss is found to be 4.1 dB. Consequently, it can be concluded that distinguishing between different types of construction materials leads to more accurate results of the path loss prediction (compared to 12.8 dB predicted by Log-normal Shadowing Model). Furthermore, model (2.11) evidently decouples free space path loss from the attenuation loss produced by physical obstacles which lie in the T-R propagation path.

2.2.2 Improved Empirical Model for Indoor Propagation Prediction

Murch et al. [1995] keep working on the improvement of radio channel models for indoor signal propagation. They are focused on improving the accuracy of the multi-wall propagation models while retaining the straightforwardness of the log-distance model computation.

In the Log-distance path loss model, additional loss is introduced for each floor and each wall that the signal is traversing, resulting in so called Multi-wall multi-floor model:

$$PL(d) = 10\log\left(\frac{d}{d_0}\right)^n + \sum_{p=1}^{P} WAF(p) + \sum_{q=1}^{Q} FAF(q) \tag{2.12}$$

Path loss PL in dB is a function of T-R separation distance d (expressed in meters). Rest of parameters are following:

d_0 is the reference distance in meters;

n is path loss index, dimensionless entity;

P and Q are number of walls and floors respectively;

$WAF(p)$ is Wall Attenuation Factor in dB for the wall of type p;

$FAF(q)$ is the Floor Attenuation Factor for the floor of type q, also in dB.

Instead of fitting the values of n, WAF and FAF empirically into the measurements, Murch et al. [1995] propose a more theoretical approach. Introducing some of the propagation phenomena suggested by Uniform geometrical Theory of Diffraction (UTD) is claimed to improve the accuracy of (2.12). Determining the parameters n, WAF and FAF from the measurement would also not necessarily be required. Additional advantage is that "the computational time of the resulting model would be kept low without a significant reduction in the accuracy of prediction" Murch et al. [1995] (compared to the UTD propagation models).

First propagation phenomena to be considered is the distance dependence of path loss. Namely, in the study of microcells, it was observed that the path loss starts to increase more rapidly beyond a certain point in space. If plotted as the function of T-R distance, path loss appears to be a dual-slope piecewise linear curve, as it is depicted in figure 2.1. The place at which the

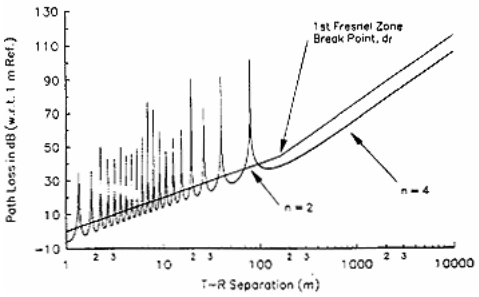

Figure 2.1. Feuerstein et al. [1994]: Illustration of a double slope path loss dependence on T-R separation

two distinct regions are separated is called the "break point", and it represents the distance at which the first Fresnel zone becomes obstructed. According to Murch et al. [1995], "the size of the first Fresnel zone a distance d from the transmitter is approximately given by $Z_f = \sqrt{\lambda d}$. Consequently in a corridor of width 1.5 m it will be obstructed at distances greater then about 5 m for frequencies around 900 MHz. In rooms where there is more clear space the first Fresnel zone will be obstructed by the ceiling or floor and this will occur at about 15 m from the transmitter. To keep our model simple we propose to simply take the average of these values and use 10 m for the break point d_bp in all situations".

As one could see in figure 2.1, the linear path loss curves after and up to the break point have different slops. This implies the distinction of the path loss indexes for both sides of the break point, namely n_1 and n_2, which strongly depend on the propagation environment. It has been said before that the new parameters are introduced in order to approve the model accuracy;

however the goal is to obtain their values through the theoretical considerations and keep the complexity of the modeling process as low as possible. Murch et al. [1995] report that n_1 value should be less than the freespace value of 2, and thus $n_1 = 1$ is proposed. Since the possible value for n_2 ranges $[2 \div 3]$, the average 2.5 is taken.

When the break point d_{bp} is consolidated into multi-wall multi-floor model (2.12), it becomes:

$$\begin{aligned} PL(d) = 10\log\left(\frac{d}{d_0}\right)^{n_1} U(d_{bp}-d) \\ + 10\left[\log\left(\frac{d_{bp}}{d_0}\right)^{n_1} + \log\left(\frac{d}{d_{bp}}\right)^{n_2}\right] U(d-d_{bp}) \\ + \sum_{p=1}^{P} WAF(p) + \sum_{q=1}^{Q} FAF(q) \end{aligned} \tag{2.13}$$

$U(\cdot)$ is the unit step function defined as:

$$U(d) = \begin{cases} 0 & d < 0 \\ 1 & d \geq 0 \end{cases} \tag{2.14}$$

Second propagation effect to be investigated is the angle dependence of the attenuation factors. Specifically, depending on the angle of incidence between the wall/floor and the electromagnetic wave, a different amount of energy is transmitted through that wall/floor. In order to quantify the former, Murch et al. [1995] have theoretically investigated the loss which can be expected for variety of different wall types. Eventually, it is concluded that "at grazing incidence the transmission is assumed to be zero, whilst at normal incidence it is equal to the value of $WAF(p)$ or $FAF(q)$ originally obtained through the propagation measurements as with (2.12); at the angles between grazing and normal incidence, the values are interpolated using a cosine function as $WAF(p)/\cos\theta_p$". The multi-wall multi-floor model (2.13) can be further expanded to:

$$\begin{aligned} PL(d) = 10\log\left(\frac{d}{d_0}\right)^{n_1} U(d_{bp}-d) \\ + 10\left[\log\left(\frac{d_{bp}}{d_0}\right)^{n_1} + \log\left(\frac{d}{d_{bp}}\right)^{n_2}\right] U(d-d_{bp}) \\ + \sum_{p=1}^{P} WAF(p)/\cos\theta_p + \sum_{q=1}^{Q} FAF(q)\cos\theta_q \end{aligned} \tag{2.15}$$

The new parameters are:

$WAF(p)$ and $FAF(q)$ are values of wall and floor attenuation factors occurring at normal incidence of the radio wave with the wall;

θ_p is the angle between the p^{th} wall and the the straight line path joining the transmitter to the receiver;

θ_q is the angle between the q^{th} floor and the the straight line path joining the transmitter to the receiver.

Ascertaining the $WAF(p)$ and $FAF(q)$ values is more difficult to be done theoretically, hence they were had to be estimated from the direct measurements and the model (2.12). For concrete block their value is 6.6 dB, and for the plaster board 2.5 dB.

Although the attenuation factors of walls and floors had to be obtained experimentally, 'Improved Empirical Model for Indoor Propagation Prediction' integrates some of important propagation phenomena from UTD and provides the means of their theoretical derivations, which finally results in small overhead of computation.

2.2.3 Through-the-Wall Propagation and Material Characterization

All previously described models that govern the use of wall and floor attenuation factors deduced their values by conducting the on-site measurements of signal penetration through the relevant walls and floors. Avoiding these measurements, if possible, would obviously reduce the complexity of the channel modeling process.

The research objective of Muqaibel et al. [2005] was to explore UWB signal propagation through the walls made of typical building construction materials and make use of the acquired data for UWB characterization of the same materials. This was done by obtaining the insertion transfer function, which is defined Muqaibel et al. [2005] as the ratio of two signals measured in the presence and in the absence of the material under test. The insertion transfer function is directly related to the loss and the dielectric constant of each material.

The measurements over $[1 \div 15]$ GHz frequency range were performed on 10 common materials found inside buildings: concrete blocks, reinforced concrete, bricks, structure wood, dry wall, wallboard, wooden door, cloth office partition, styrofoam slab and glass sheet. Graphical and numerical results for the dielectric constant and the loss of previous materials are given in Muqaibel et al. [2005] as lookup tables. The authors are encouraging the use of data for studying channel modeling problems.

Some of tables which contain values required for radio channel simulation in this thesis are given below.

For ply wood:

Frequency [GHz]	**Loss [dB]**	**Dielectric Constant**	**Attenuation [dB/m]**
2.00	1.27	2.55	48.68
2.70	1.40	2.57	61.07
3.40	1.52	2.57	73.46
4.10	1.65	2.56	85.84
4.80	1.77	2.55	98.23
5.50	1.89	2.56	110.62
6.20	2.02	2.52	123.01
6.90	2.14	2.51	135.40
7.60	2.26	2.49	147.79
8.30	2.39	2.48	160.18
9.00	2.51	2.46	172.57
9.70	2.64	2.45	184.95

Frequency [GHz]	Loss [dB]	Dielectric Constant	Attenuation [dB/m]
10.40	2.76	2.44	197.34
11.10	2.88	2.42	209.73
11.80	3.01	2.41	222.12
12.50	3.13	2.40	234.51
13.20	3.26	2.38	246.90
13.90	3.38	2.37	259.29
14.60	3.50	2.35	271.68

Table 2.1. Muqaibel et al. [2005] Measurements of RF signal loss through ply wood

For a single brick:

Frequency [GHz]	Loss [dB]	Dielectric Constant
1.01	2.06	3.73
1.31	2.38	3.70
1.61	2.70	3.71
1.91	3.02	3.74
2.21	3.34	3.78
2.51	3.66	3.82
2.81	3.98	3.86
3.11	4.30	3.90
3.41	4.62	3.94
3.71	4.95	3.98
4.01	5.27	4.02
4.31	5.59	4.07
4.61	5.91	4.11
4.91	6.23	4.16
5.21	6.55	4.20
5.51	6.87	4.25
5.81	7.19	4.29
6.11	7.51	4.34
6.41	7.84	4.39
6.71	8.16	4.43
7.01	8.48	4.48

Table 2.2. Muqaibel et al. [2005] Measurements of RF signal loss through a single brick

2.3 Radio Irregularity Model

All previously described log-distance models, (2.3), (2.7), (2.9), (2.11) and (2.15), are referred to as spherical radio models. Spherical radio model assumes the wavefronts are spheres and the wave propagates radially outward Barclay [2002], meaning that the signal attenuates equally in all directions. This model is commonly used by wireless network simulators, such is Zeng et al. [1998], but unfortunately it is not accurate enough. This was proven in Zhou et al. [2004], by researchers who used MICA2 wireless sensor nodes to experimentally validate the existence of the radio irregularity phenomena and investigate its impact on the communication performance in WSN. Experimental results confirm that "radio propagation is largely non-isotropic and exhibits a continuous variation with incremental changes in direction" Zhou et al. [2004].

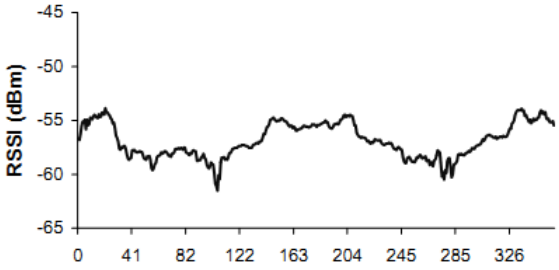

Figure 2.2. Zhou et al. [2004]: Received signal strength values in different directions

Figure 2.2 shows "the variation of received signal strength as a function of the angular direction with respect to the sender" Zhou et al. [2004]. The signal strength was recorded within MICA2 receiver which made a circular shift around MICA2 transmitter while keeping the distance between them constant. Radio irregularity is a non-negligible effect which occurs in wireless communications - its impact on MAC and routing protocols is thoroughly analyzed in Zhou et al. [2004].

Two causes of radio irregularity are reported: a non-isotropic properties of the propagation media and heterogeneous properties of sensor devices. The appearance of scattering, diffraction and reflection in the communication media (which are the inevitable side effects of wireless signal propagation) lead to the significant variation of signal's path loss. Heterogeneous properties of sensor nodes may emerge from the manufacturing process, thus the same types of nodes may transmit radio signals with different sending powers. The batteries play an important roll as well, since they get discharged with different rates after the initial deployment of WSN. All of the previously described effects give rise to the radio irregularity phenomena which is the main cause of asymmetric radio interference. In Zhou et al. [2004], a Radio Irregularity Model (RIM) is derived, which is an extension of isotropic radio models of the form:

$$Received\ Signal\ Strength = Sending\ Power - Path\ Loss \tag{2.16}$$

Using the data empirically obtained from MICA2 wireless sensor nodes, the authors formulated RIM model, which is "the first to bridge the discrepancy between spherical radio models used by simulators and the physical reality of radio signals".

To quantify the impact of radio irregularity, a Degree of Irregularity (DOI) is defined as "the maximum received signal strength percentage variation per unit degree change in the direction of radio propagation". As seen in figure 2.3, when DOI value is set to zero the propagation is considered as isotropic. But as the value becomes higher, the radio range variation takes more effect.

Figure 2.3. Zhou et al. [2004]:Degree of Irregularity

To account for the non-isotropic property of radio irregularity (and irregularity's continuous variation), the path loss value is adjusted with the DOI:

$$Received\ Signal\ Strength = Sending\ Power - Path\ Loss * K_i \tag{2.17}$$

The coefficient K_i represents the path loss change in different directions. It is calculated based on formula

$$K_i = \begin{cases} 1 & i = 0 \\ K_{i-1} \pm Rand * DOI & 0 < i < 360 \quad \wedge i \in N \end{cases} \tag{2.18}$$

where $|K_0 - K_{359}| \leq DOI$. 360 different K_i values could be therefore obtained for 360 spacial directions. The starting direction, K_0, is randomly fixed. It is reported in Zhou et al. [2004] that statistical analysis of experimental data shows the best fit of received signal strength variation for Weibull distribution. Accordingly, a random number $Rand$ is generated according to the Weibull distribution. The DOI value should be calculated in line with its definition.

When it comes to differences among devices' hardware calibration and battery statuses which result in heterogeneous sending powers, second parameter is introduced to portray this impact on radio irregularity. Variance of Sending Power (VSP) is defined as the maximum percentage variance of the signal sending power among different devices. Assuming the variance of sending power follows Normal distribution, VSP is modeled as following:

$$VSP\ Adjusted\ Sending\ Power = Sending\ Power * (1 + Rand * VSP) \tag{2.19}$$

Finally, incorporating both DOI and VSP parameters into isotropic radio model (2.16), the Radio Irregularity Model outcomes:

$$\begin{aligned} Received\ Signal\ Strength = {} & VSP\ Adjusted\ Sending\ Power \\ & - DOI\ AdjustedPath\ Loss \end{aligned} \tag{2.20}$$

Previous model portrays the real case of radio signal propagation and it is obviously preferable for use in simulators rather than isotropic models. The impact of radio irregularity on MAC layer to smaller extent and on routing to large extent may be found in Zhou et al. [2004].

Chapter 3

Problem Statement

"Modeling the radio channel has historically been one of the most difficult parts of mobile radio system design."

Theodore S. Rappaport

The 'Improved Empirical Model for Indoor Propagation Prediction' (2.15) intended for use in multi-wall and multi-floor environments provides various opportunities for investigation of its parameters and their impact on wireless signal propagation. First goal of this work was therefore to simulate the prediction of path loss according to this model and find the most suitable scenarios to investigate its parameters. For the sake of simplicity and in order to best explore the influences of this parameters on the propagation of wireless signal, it was decided to perform simulation of the case when only one wall is placed between the receiver and the transmitter. Hence the 'Improved Empirical Model for Indoor Propagation Prediction' (2.15) can be slightly modified to fit this specific purpose as in equation (3.1):

$$\begin{aligned} PL(d) = {} & 10\log\left(\frac{d}{d_0}\right)^{n_1} U(d_{bp}-d) \\ & + 10\left[\log\left(\frac{d_{bp}}{d_0}\right)^{n_1} + \log\left(\frac{d}{d_{bp}}\right)^{n_2}\right] U(d-d_{bp}) \\ & + \frac{WAF}{\cos\theta} \end{aligned} \tag{3.1}$$

In previous equation, the Floor Attenuation Factors FAF are excluded and the sum of Wall Attenuation Factors WAF is simplified for the case when only one wall is found in T-R distance, $WAF/\cos\theta$.

Furthermore, if path loss predicted by (3.1) is embedded into Radio Irregularity Model (2.20), realistic and more accurate results are expected to be obtained in simulation. The repercussion of radio irregularity on MAC and routing layers is comprehensively analyzed and described in Zhou et al. [2004], however its influence on physical layer is apparent from simulation results. This is the additional observation made from simulation.

Simulation of wireless signal propagation through one wall has been implemented in MATLAB and experimentally verified by performing the measurements using TelosB wireless sensor nodes.

Second goal of this work was to thoroughly investigate the influence of WAF onto wireless signal attenuation. As mentioned in previous chapter, for empirical path loss models the values of WAF are found experimentally and optimized to best fit these models. They do not take into consideration the thickness of walls and floors. Here, the idea was to make use of data collected by Muqaibel et al. [2005] (described in section 2.2.3 , tables 2.1 and 2.2) and calculate the proper value of attenuation factor (signal loss) for particular type and thickness of wall, which also depends on signal's frequency. Obtaining the values of WAF from predetermined tables instead of turning to on-site measurements and optimization techniques represents a significant reduction in complexity of the indoor propagation modeling process.

Moreover, the difference between two types of walls was closely examined and proved to exist experimentally. Measurements have been carried out for wooden and brick walls at the campus of Università della Svizzera italiana.

Chapter 4

Measurements of Radio Irregularity

Using a pair of MICA2 wireless sensor nodes for their experiments, Zhou et al. [2004] successfully demonstrated the presence of radio irregularity phenomena and gave the formal definition of Degree Of Irregularity (DOI) in Radio Irregularity Model: *DOI is the maximum received signal strength percentage variation per unit degree change in the direction of radio propagation*. In this thesis TelosB nodes were used for conducting the measurements of received signal strength in 360 degrees, by repeating the experiment as described in Zhou et al. [2004]. The data is afterwards used for the calculation of required DOI value.

TelosB is an ultra low power sensor node with 2.4 GHz IEEE 802.15.4 Chipcon Wireless Transceiver. Specifically, Chipcon CC2420 radio has a programmable output power. TelosB node provides a digital Received Signal Strength Indicator (RSSI), whose value is represented as the 8-bit signed 2's complement cc2. This value, RSSI_VAL, can be referred to the received signal's power P at the RF pins using the following equation:

$$P = RSSI\_VAL + RSSI\_OFFSET \ [dBm] \tag{4.1}$$

where RSSI_OFFSET equals -45 and is empirically obtained during system development from the front and gain cc2. Consequently, upon the completed experiment all the received signal strength data read out from node's internal memory has been interpreted in signed 2's complement representation and the overhead of 45 was subtracted before further processing and analysis of results.

Sensor nodes make use of integrated omnidirectional Inverted-F antenna to send radio signals. The antenna's radiation patterns, provided by Chipcon AS, could be found in tel.

The TelosB platform features TinyOS support - TinyOS is an open-source software operating system developed by the University of California, Berkeley. TinyOS is written is nesC programming language, a component-based dialect of C, which is specifically targeted for low-power wireless devices and optimized for their memory limits. TinyOS programs are implemented by means of software components, the discrete units of functionality; the components are connected ('wired') to each other using interfaces. The operating system is making use of levels of hardware abstraction.

For the purpose of DOI measurements, a pair of TelosB nodes was programmed to establish the radio communication. The experiment was carried out inside the Main Building of Università della Svizzera italiana, in Lugano, Switzerland. The experimental setup is shown in figure 4.1. The receiver Rx made a full circle around the transmitter Tx which was placed in its center. The circle was drawn around the transmitter using a piece of chalk and the rope, such to form 2 m semi-diameter from the center. Starting from degree 0, the receiving node was consequently moved to 359 equidistant positions on the circle in order to receive each of 360 packets sent by the sending node. The transmitter's output power was kept minimal. At the other side, the packets received at Rx node were stored in its internal memory along with the values of received signal strength in dBm (read out from node's RSSI registers). These values were later transferred to PC via USB serial communication and processed in accordance with 4.1, as described before in this section.

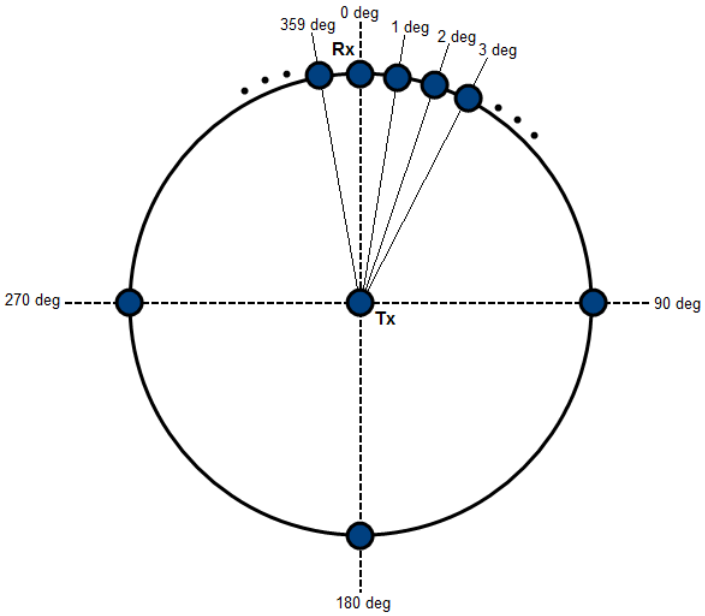

Figure 4.1. DOI experimental setup. The sending TelosB Tx node has sent 360 messages which were received by receiver Rx at 360 equidistant positions in the circle. The circle with 2 m semi-diameter, which is also the constant T-R separation distance, was drawn on the floor fixing one side of 2 m rope in the center and pulling the piece of chalk fixed at the other end while keeping the rope firmly tighten.

As explained in State of the Art chapter, one of the parameters which configure in Radio Irregularity Model 2.20 is the Variance of Sending Power (VSP). Since in this experiment only 2 wireless nodes were used, the voltage of their batteries was checked with a multimeter immediately before and after the experiment. It was observed that the voltage level decreased from 1.606 V to 1.605 V. Thus, it can be concluded that the maximum percentage variance of the signal sending power among 2 different devices is 0.062 %, which is negligibly small and may be ignored.

The received signal strength values recorded at Rx node are shown in figure 4.2. The plot undoubtedly proves the non-negligible presence of radio irregularity phenomena and confirms its continuous variation with incremental changes in direction, as suggested by Zhou et al. [2004]. The same results are displayed in figure 4.3, as to credibly portray the non isotropic radio wave propagation and irregular radio pattern. The measurement results mirror as well what happens in reality when the antennas are not ideally omnidirectional.

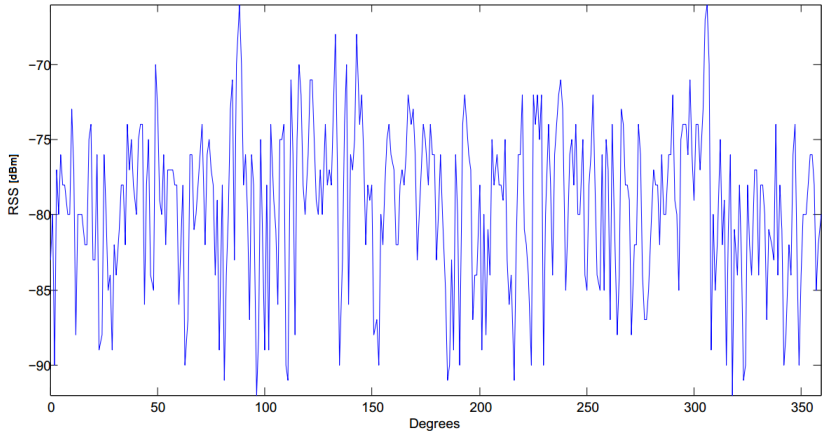

Figure 4.2. The measured received signal strength variation with respect to different angular direction

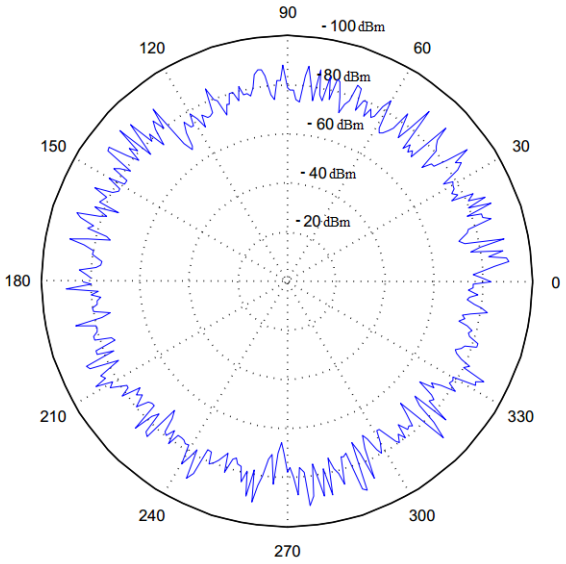

Figure 4.3. Irregularity of the radio pattern

Having the empirically obtained data, DOI value can be calculated according to its definition: the maximum percentage difference among adjacent received signal strength values was

adopted as the degree of irregularity. For the indoor environment of Università della Svizzera italiana, DOI = 0.247.

The radio irregularity's significant impact on connectivity, interference, asymmetric links and protocol performance in wireless networks is thoroughly explored in many articles Muetze et al. [2008], Bettstetter and Hartmann [2005], Hekmat and Van Mieghem [2006], Zhou et al. [2006], De Marco et al. [2007]. The variation of received signal strength in different directions for the same T-R separation directly leads to different path loses in different directions. The irregularity effect should be therefore captured for the sake of accurate simulations of wireless network systems, and thus performing the measurements and collecting the empirical data required for DOI calculation is a payable effort.

Chapter 5

Wall Attenuation Measurements

Before proceeding with the measurements of signal loss through the specific walls, it is firstly necessary to establish and analyze possible measurement scenarios which will further be simulated in MATLAB. The measurement scenarios depend heavily upon model's parameters, hence they should be examined first and their values should be determined.

As clarified in Chapter 3 - Problem Statement, this work uses the empirical model (2.15) in a slightly modified form to fit the case of signal propagation through a single wall:

$$\begin{aligned} PL(d) = {} & 10\log\left(\frac{d}{d_0}\right)^{n_1} U(d_{bp}-d) \\ & + 10\left[\log\left(\frac{d_{bp}}{d_0}\right)^{n_1} + \log\left(\frac{d}{d_{bp}}\right)^{n_2}\right] U(d-d_{bp}) \\ & + \frac{WAF}{\cos\theta} \end{aligned} \tag{5.1}$$

The output of the model is path loss PL which is a function of T-R separation distance d. The reference distance d_0 must be chosen so to lie within transmitter's far filed. Rappaport [2001] states that the reference distance for antennas in 2 GHz region is typically chosen to be 1 m for indoor environments. The next parameter to be considered is the break point distance d_{bp}. Unfortunately, no clear explanation is provided by Murch et al. [1995] regarding the exact methodology used to derive the value of 10 m for the break point distance. Therefore, it has been necessary to seek for additional definitions.

5.1 The break point distance

Feuerstein et al. [1994], Barclay [2002] and Xia et al. [1993] define the break point as the distance for which the ground begins to obstruct the first Fresnel zone. For the line-of-sight topologies, the first Fresnel zone corresponds to an ellipsoid whose foci are transmitting and receiving antennas, where it holds that the sum of distances from both antennas to a point on

the ellipsoid is $\lambda/2$ greater then the T-R direct distance Feuerstein et al. [1994], figure 5.1. This is known as the 2-ray model for the flat earth. The break point is the distance at which the first Fresnel zone touches the ground.

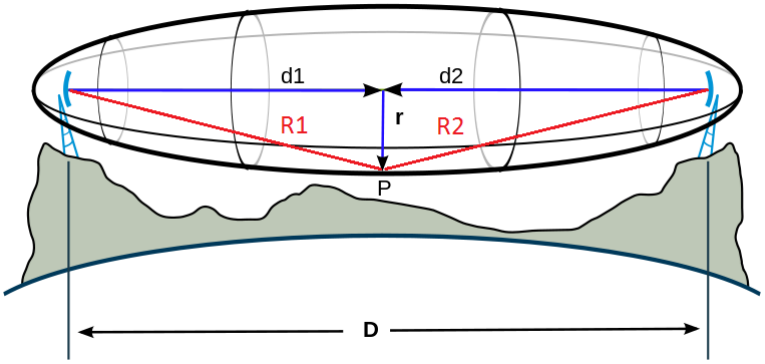

Figure 5.1. First Fresnel zone in 2-ray model for the case of flat earth, wik [a]. D - distance between the transmitting and receiving antennas (T-R separation distance); r - size of the first Fresnel zone in point P; $R1$ and $R2$ - distances from transmitting and receiving antennas to the point P in ellipsoid, respectively. For the first Fresnel ellipsoid the equation $R1+R2=D+\lambda/2$ holds, where λ is the transmitted signal's wavelength.

In the first region, prior to the break point, the propagation path is said to have first Fresnel zone clearance since there is only free space path loss. But once the Fresnel zone is obstructed (by ground), the signal strength becomes sorely attenuated and thus different path loss exponents are valid in different distance regions (this propagation effect is precisely captured in figure 2.1). Measuring the values of these indexes has been a subject of research in many scientific publications. As they are obtained through extensive measurements inside the buildings, there are plenty of results published. They vary based on the building type and construction materials, as well as the frequency of the propagated radio signal Nikookar and Prasad [2009].

Consequently, according to the Fresnel zone model, for high frequency signals the distance at which the first Fresnel zone touches the ground is calculated as Barclay [2002], Xia et al. [1993]:

$$d_{bp} = \frac{4h_t h_r}{\lambda} \tag{5.2}$$

where h_t and h_r correspond to the transmitting and receiving antenna heights in meters, respectively.

Different values for path loss exponents are reported in the literature, most of which were obtained empirically. In case of indoor high frequency radio propagation, Nikookar and Prasad [2009] and Feuerstein et al. [1994] suggest $n_1 = 2$ for the first region up to the break point. For distances higher than d_{bp}, n_2 ranges from 2 to 7 Nikookar and Prasad [2009].

Putting it all together, the break point distance can be calculated straight forward from (5.2). As regards of values for n_1 and n_2, in the aim of finding the best fit that matches measured data, the idea is to fix the value of n_2 first and run the simulation for a range of n_1 values - this way its influence on the propagation could be analyzed. Afterwards n_2 will be alternated while keeping n_1 fixed to the most suitable value discovered from the first simulation.

Further analysis of model (5.1), suggests the two cases could be distinguished based on the position of the break point. The line of sight between the transmitter and the receiver will be disrupted anyhow by the presence of the wall. However, assuming there is no wall, the point at which the first Fresnel zone would touch the ground - the break point - can be determined, according to formula (5.2). If the break point occurs before the wall (i.e. first Fresnel zone touches the ground before the wall), it makes sense to consider two separate free space propagation regions with different path loss indexes, as discussed above. But in case the break point occurs after the wall, penetration through the wall would result in different attenuation of signal strength, which is not due to free space anymore.

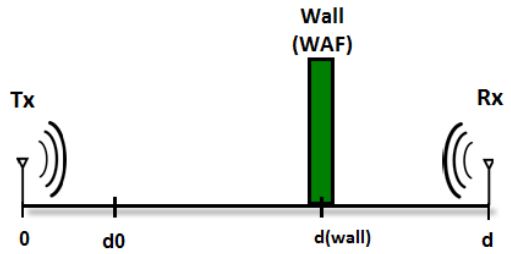

(a) Simulation scenario 1. When calculated, the break point distance d_{bp} will be larger than the distance of the wall d_{WALL}, i.e. the break point would occur after the wall. Hence, according to Fresnel zone theory, it does not make sense to incorporate its effect on signal propagation in this case.

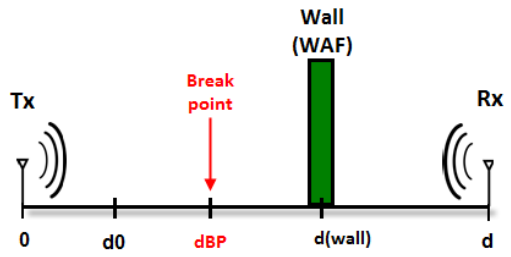

(b) Simulation scenario 2. In this scenario the break point will fall prior to the wall, i.e. $d_{bp} < d_{WALL}$. Due to the loss of first Fresnel zone clearance, signal path loss will significantly increase - for this reason free space propagation up to the wall will have two segments, characterized by different path loss indexes.

Figure 5.2. Simulation scenarios

Therefore, (5.1) can be rewritten as:

$$\text{if } d < d_{bp}: \quad PL(d) = n_1 10\log\left(\frac{d}{d_0}\right) + \frac{WAF}{\cos\theta}$$

$$\text{if } d > d_{bp}: \quad PL(d) = n_1 10\log\left(\frac{d_{bp}}{d_0}\right) + n_2 10\log\left(\frac{d}{d_{bp}}\right) + \frac{WAF}{\cos\theta}$$

The first case when $d < d_{bp}$ is illustrated in figure 5.2a. The wall is placed before the break point distance and thus the model accounts for free space propagation (characterized with path loss index n_1) up to the receiver's distance d, on the top of which the Wall Attenuation Factor WAF is added to model the loss induced by wall. In second case when $d > d_{bp}$, portrayed in figure 5.2b , the break point distance d_{bp} is less than distance of the wall $d(wall)$ (relative to the transmitter's position, 0). This time the model incorporates the situation when Fresnel zone touches the ground: there are two propagation regions defined by different path loss indexes n_1 and n_2. The WAF is also added to comprise the wall loss.

5.2 Wall Attenuation Factor

Since one of the goals in this work was to explore the influence of the wall on signal propagation and especially the quantity of attenuation introduced by the wall, a sending Tx node will be placed from one side of the wall while five receiving nodes Rx 1-5 will record the received signal strength on the other side. The reason for having five receivers is to make an observation if the angle of penetration contributes to the amount of attenuation as predicted by model 2.15.

The angle between the wall and direction of electromagnetic signal propagation can be obtained as detailed in figure 5.3.

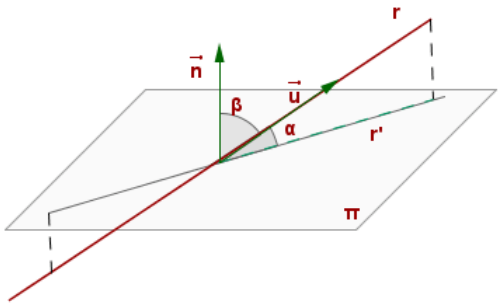

Figure 5.3. The angle between the line and plane. The angle between a line r and a plane π is the angle between r and its orthogonal projection r' onto π. In this case it is angle α.

The angles of incidence between the wall and the electromagnetic waves, θ, will be set up to be 45°, 30°, 0°, 30° and 45°, respectively in measurements. In order to investigate the influences of break point and wall attenuation factor as clearly as possible, T-R separation distances for all five receivers will be fixed to the same value, not to interfere. The transmitter and the

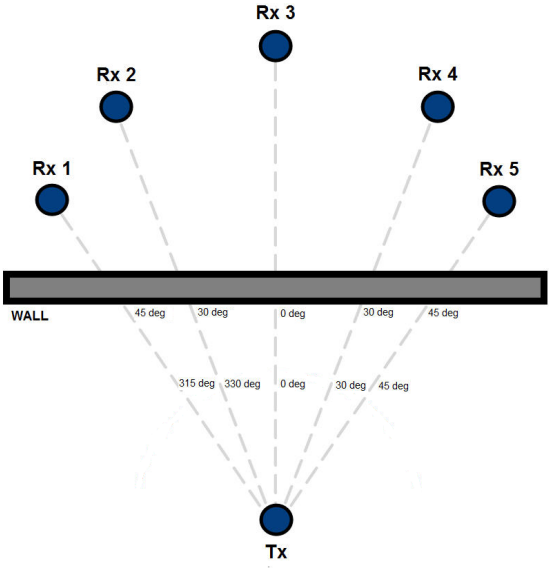

(a) Scenario 1. The break point is beyond the wall and therefore not relevant for the model

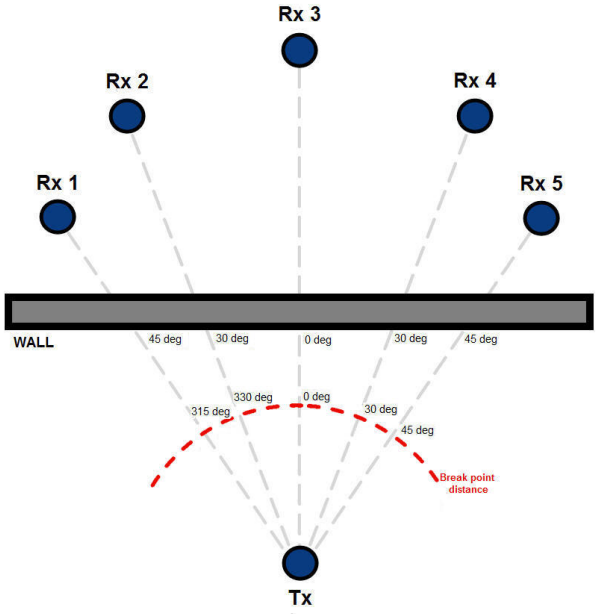

(b) Scenario 2. The break point is prior to the wall and its effect is considered in the model

Figure 5.4. Two simulation scenarios and measurement setups based on model 5.1

receivers will be placed at the same height (on the top of carton boxes) in measurements, which will make easier calculation of angles between the straight line joining each receiver to the transmitter and the wall.

One additional explanation regarding aforementioned angles must be given here. By means of radio irregularity phenomena, the angles will be used in a slightly different manner in MATLAB simulation. If one recalls of the Radio Irregularity Model and equation (2.17) in particular, it becomes clear that the angles of the receivers' directions with respect to the sender will be 315°, 330°, 0°, 30° and 45° when the spherical propagation of signal around the receiver is considered. More detailed explanation on former will be given in Chapter 6 - Simulation in MATLAB. Both previous values and the values of wall penetration angles θ are outlined in figure 5.4.

Incorporating the concept of having five receivers into previously described scenarios, 5.2, yields the final two simulation scenarios according to which the measurement setups may be established. The two cases are represented in figure 5.4 .

5.3 The measurements

Using the TelosB wireless sensor nodes and based on scenarios shown in figure 5.4 , radio signal measurements were performed for two types of walls: a brick wall in between the classrooms at the main building of Università della Svizzera italiana, and a wooden wall inside the office of University's Executive center. The thickness of the brick wall is 15 cm, and 12 cm of the wooden wall.

Sensor nodes are put on the top of carton boxes 26 cm in height. Applying (5.2), the break point distance was determined:

$$d_{bp} = \frac{4h_t h_r}{\lambda} = \frac{4 \cdot 0.26 \cdot 0.26}{0.125} = 2.16m \tag{5.3}$$

In order to fit the scenarios, T-R separation distance d is chosen to be 1.9 m for the first case (Scenario 1), and 3.5 m for the second case (Scenario 2).

Knowing the operating frequency of TelosB platform is $f = 2.4\ GHz$, the wavelength of transmitted radio signal, λ, was calculated using

$$\lambda = \frac{c}{f} = \frac{3 \cdot 10^8}{2.4 \cdot 10^9} = 0.125m \tag{5.4}$$

where $c = 3 \cdot 10^8\ \frac{m}{s}$ is the speed of light.

Total time of radio transmission (total time of measurements) for both scenarios was 15 minutes, with packets sent every 20 ms. The RSSI readings stored in the internal memories of TelosB wireless sensor nodes were transfered to the PC via serial USB communication after every measurement run, and the memories have been cleared to store the new batch. The data has been processed in MATLAB. The plot of mean values for both walls is represented in figure 5.5.

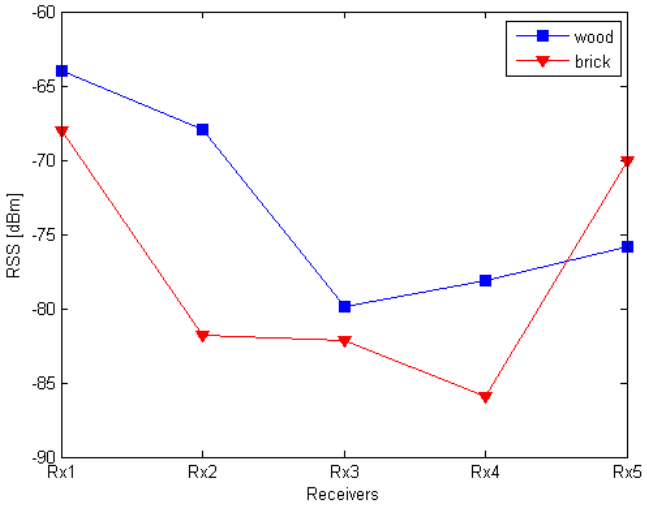

Figure 5.5. The mean received signal strength for 2.4 GHz signal propagation through the wooden and brick walls

The number of packets received at each of five receivers together with the mean values of received signal strength, standard deviation and variance are listed in tables below.

Wooden wall					
	Rx1	**Rx2**	**Rx3**	**Rx4**	**Rx5**
Number of packets received	30604	30614	30595	30586	30605
Mean RSS [dBm]	-75.7905	-78.1006	-79.8489	-67.9476	-63.9861
Standard deviation [dBm]	0.6507	0.4575	0.5541	0.2277	0.1223
Variance	0.4234	0.2093	0.3070	0.0518	0.0150

Table 5.1. Wooden wall: Number of packets received, mean, standard deviation and variance of received signal strength

Brick wall					
	Rx1	**Rx2**	**Rx3**	**Rx4**	**Rx5**
Number of packets received	30587	30614	30395	30617	30607
Mean RSS [dBm]	-70.0032	-85.9236	-82.1420	-81.7999	-68.0030
Standard deviation [dBm]	0.0779	0.5549	0.4058	0.4163	0.0680
Variance	0.0061	0.3079	0.1647	0.1733	0.0046

Table 5.2. Brick wall: Number of packets received, mean, standard deviation and variance of received signal strength

Given the standard deviation σ which is, same as mean, expressed in dBm, it is possible to compute the ϵ neighborhood as $mean \pm \sigma$. In order to better show the accuracy of measurements, table 5.3 gives the percentage of received signal strength values which lie within the ϵ neighborhood.

	Rx1	**Rx2**	**Rx3**	**Rx4**	**Rx5**
Wooden wall	85.0836%	87.3718%	81.6604%	94.8767%	98.6211%
Brick wall	99.4802%	74.0576%	86.1359%	79.9588%	99.7713%

Table 5.3. The percentage of measured received signal strength values lying within the $mean \pm \sigma$ region

Based on previous results, it can be stated with high confidence that the brick wall introduces higher amount of attenuation with respect to the wooden wall, which is in line with the initial assumptions.

Chapter 6

Simulation in MATLAB

A script was made in MATLAB which simulates both cases of measurements simultaneously for wooden and brick wall. Essentially, the path loss is computed in accordance with (5.1), which is later on embedded into the RIM model (2.20). The results of computed received signal strength are plotted versus the measured values. The rest of this section gives an overview of implementation of the simulation in MATLAB together with the interpretation of results.

6.1 Computation of required parameters and their values

As explained in Chapter 5 - Wall Attenuation Measurements, having a formula for the break point distance d_{bp} (which turns out to be 2.16 m for the transmitter and receiver heights setup in measurements), different values of path loss indexes n_1 and n_2 have been simulated in order to achieve the best fit with measured values in both cases:

$$\text{if } d < d_{bp}: \quad PL(d) = n_1 10 \log\left(\frac{d}{d_0}\right) + \frac{WAF}{\cos\theta}$$

$$\text{if } d > d_{bp}: \quad PL(d) = n_1 10 \log\left(\frac{d_{bp}}{d_0}\right) + n_2 10 \log\left(\frac{d}{d_{bp}}\right) + \frac{WAF}{\cos\theta}$$

The path losses are firstly calculated for five θ angles: 45°, 30°, 0°, 30° and 45° (figure 5.4). The distance d between the transmitter and the receivers is same in each case.

The reference distance d_0 is chosen to be 1 m. The Wall Attenuation Factors (WAF) are intended to be calculated based on data found in tables 2.1 and 2.2. Regarding the 12 cm thick wooden wall, if one refers to 'Attenuation [dB/m]' column in table 2.1 , for 2.4 GHz (which is the operating frequency of TelosB wireless sensor nodes) $WAF = 7.3284$ is easily obtained by means of simple proportion. However, when trying to do the same for the value of 15 cm thick brick wall, one may notice that in table 2.2 column 'Attenuation [dB/m]' does not exist. This is explained in Muqaibel et al. [2005]: as the brick being non-homogeneous material, it

is not possible to provide attenuation coefficients measured in dB/m. Table 2.2 provides only the values of 'Loss'. For 2.4 GHz this turns out to be less then *WAF* computed for wooden wall, which is not in agreement with the results gained through the measurements that prove higher amount of attenuation for brick wall. Since obtaining the value of WAF for brick wall unfortunately could not be done, MATLAB simulation was performed only for the wooden wall.

Next, coefficients K_i have to be computed for all five angular directions: 315°, 330°, 0°, 30° and 45°, in order to adjust the path loss as the Radio Irregularity Model (RIM) indicates (2.20). Zhou et al. [2004] provided means of K_i calculation, (2.18):

$$K_i = \begin{cases} 1 & i = 0 \\ K_{i-1} \pm Rand * DOI & 0 < i < 360 \quad \wedge i \in N \end{cases} \tag{6.1}$$

where $|K_0 - K_{359}| \leq DOI$. Degree of Irregularity (DOI) has been obtained through the measurements described in Chapter 4 - Measurements of Radio Irregularity; DOI = 0.247. The random number from Weibull distribution, *Rand*, is generated in MATLAB using wblrnd function. This function takes two parameters as input arguments, a scale and a shape parameter. Namely, previous parameters are retrieved from received signal strength measurements in 360 directions, by employing another MATLAB function - wblfit.

To model the non isotropic wireless signal propagation, the logarithmic part of path loss equation (5.1) (representation of free space propagation) was multiplied with a corresponding coefficient K_i, on the top of which the WAF is added.

The Received Signal Strength (RSS) is further computed by subtracting the path loss from the transmitter's sending power:

$$RSS = Sending\ Power - Path\ Loss \tag{6.2}$$

Sending power equals -25 mW, conforming to TelosB data-sheet.

Completing the RIM model (2.20) requires one last adjustment: inclusion of Variance of Sending Power (VSP). Likewise in Chapter 5 - Wall Attenuation Measurements, VSP gathered through sensors' battery level readings can be neglected.

In the end, final propagation model to be used for simulations is as follows:

Case 1:

$$RSS = Sending\ Power - \left[10 \log \left(\frac{d}{d_0} \right)^{n_1} * K_i + \frac{WAF}{\cos \theta} \right] \tag{6.3}$$

Case 2:

$$RSS = Sending\ Power - \left[\left(10 \log \left(\frac{d_{bp}}{d_0} \right)^{n_1} + 10 \log \left(\frac{d}{d_{bp}} \right)^{n_2} \right) * K_i + \frac{WAF}{\cos \theta} \right] \tag{6.4}$$

Simulation of received signal strength for two scenarios, each having one transmitter at one side of the wall and five receivers at the other, has been done for 500 packets. In each of 500 runs a new set of K_i random coefficients was generated.

6.2 Results of simulations

Results of simulation for different path loss index n_1 are shown in figure 6.1 and for different path loss index n_2 in figure 6.2. Both n_1 and n_2 are simulated while keeping the other one fixed together (as well as the rest of parameters in model), in order to closely examine its effect on the overall result.

In respect of n_1 simulation, $n_2 = 4$ is decided to be retained according to the values stated in Nikookar and Prasad [2009]. From the figure 6.1 it is evident that suggested value of 2 in model does not meet the measured values. The increase of n_2 gradually but slowly changes the final result, and thus it can be concluded that alternation of this parameter does not have greater significance on the final result. The same occurs in simulation of n_2. This time n_1 is kept fixed at 3. In the first case, figure 6.2a , when $d < d_{bp}$, n_2 is not present in equation (6.3) hence the simulation will yield the same outcome. In second case, figure 6.2b shows the highest value of $n_2 = 8$ gives the best approximation.

Considering previous conclusions, a question rises whether the value of WAF for wood, obtained from table 2.1, is conceivable. Might be the case this value is realistically higher, rather than path loss index n_2 being so large. However, regardless of trustworthy values for n_1, n_2 and WAF, first very obvious observation draws one's attention: looking into curves in both figures 6.1 and 6.2, it becomes evident the results of MATLAB simulation are exactly the opposite of measurements (i.e. the convexities of simulation and measurement curves are opposite to one another).

The percentage difference between the results of measurements and simulation results for different values of path loss index n_1 is given in tables 6.1 and 6.2. The same percentage difference for path loss index n_2 is shown in tables 6.3 and 6.4. Due to high dispersion of measured values, for the same value of n_1 or n_2 variation of received signal strength percentage difference among receivers Rx1 - Rx5 will be tremendous.

With respect to simulation results, further analysis of model (5.1) poses the following unsolved challenges:

1. Disparity between simulation and measurements is enormous.
2. The impact of break point distance and its use in (5.1) is unclear.
3. Although it is based on log-distance path loss law (2.7), model (5.1) does not take into consideration the reference path loss $PL(d_0)$, i.e. a free space propagation from the transmitter up to the reference distance d_0.

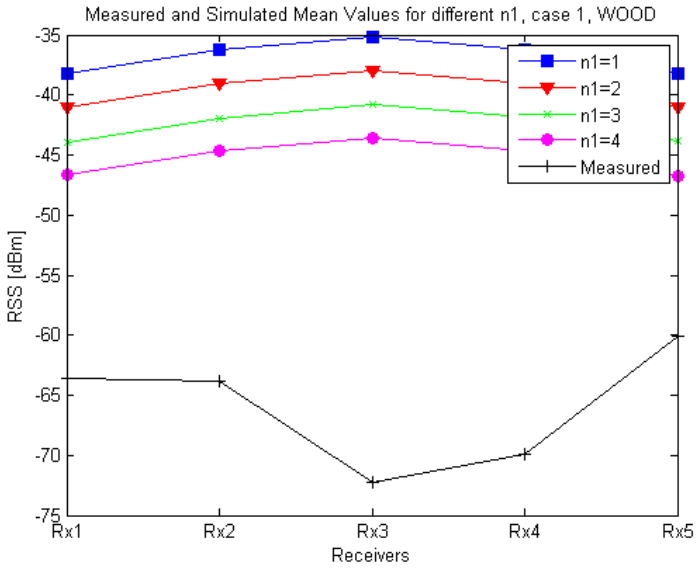

(a) Measured versus simulated received signal strength for different n1, Scenario 1

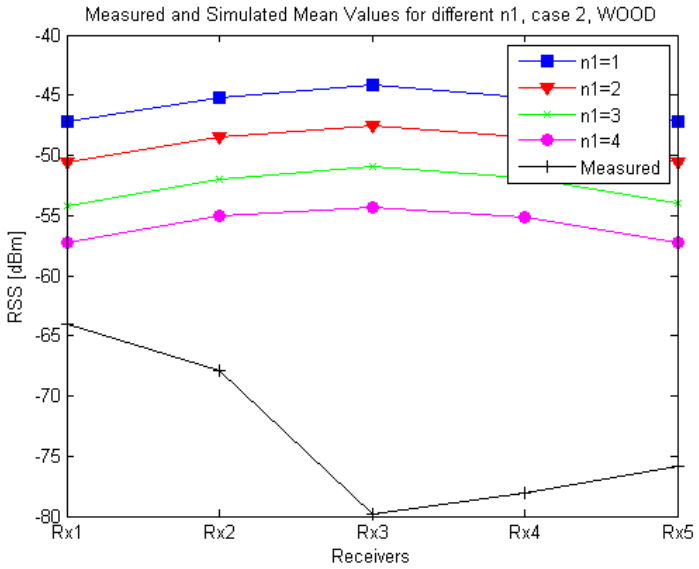

(b) Measured versus simulated received signal strength for different n1, Scenario 2

Figure 6.1. Simulated received signal strength for different values of n1

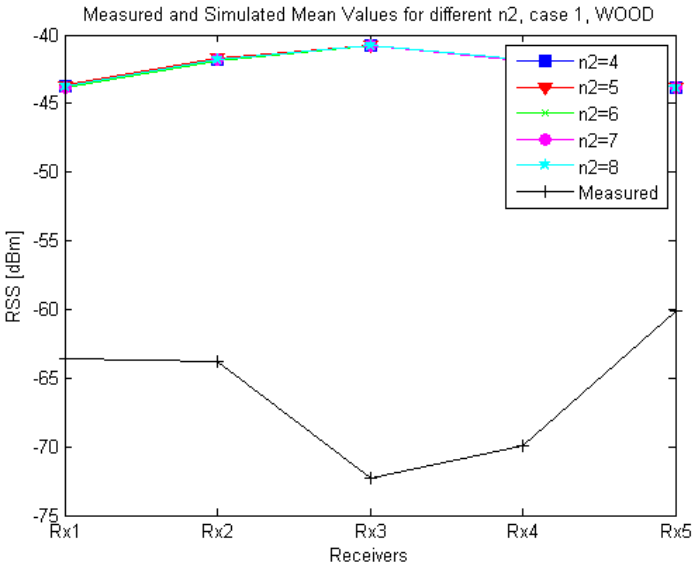

(a) Measured versus simulated received signal strength for different n2, Scenario 1

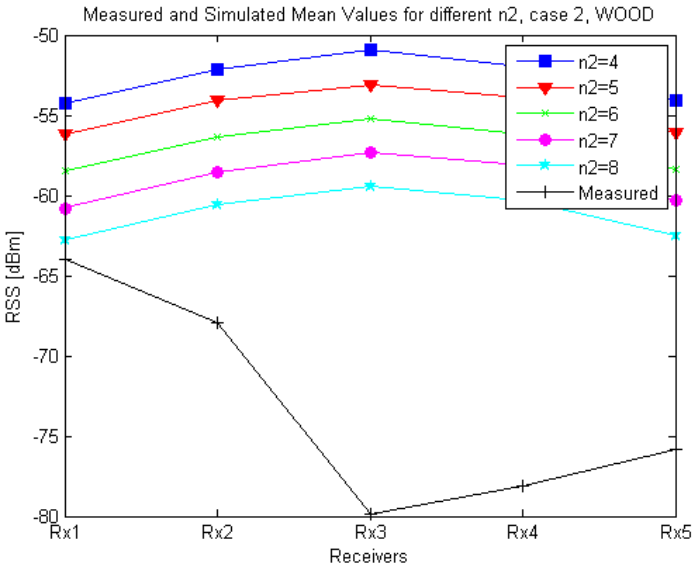

(b) Measured versus simulated received signal strength for different n2, Scenario 2

Figure 6.2. Simulated received signal strength for different values of n2

	Rx1	**Rx2**	**Rx3**	**Rx4**	**Rx5**
n_1=1	49.8525%	55.0471%	69.0855%	63.4439%	44.5571%
n_1=2	43.2149%	48.2615%	62.1910%	56.7525%	37.7838%
n_1=3	36.6739%	41.5346%	55.6490%	50.3226%	31.2505 %
n_1=4	30.4915%	35.2660%	49.4429%	44.1003%	24.9983%

Table 6.1. Percentage difference between measurement results and simulation results for different path loss index n_1, Scenario 1

	Rx1	**Rx2**	**Rx3**	**Rx4**	**Rx5**
n_1=1	29.8925%	39.9763%	57.4675%	53.4278%	46.3684%
n_1=2	23.1632%	33.1818%	50.6177%	46.6778%	39.8183%
n_1=3	16.5035%	26.3860%	44.1156%	40.4259%	33.6390 %
n_1=4	10.6831%	20.4883%	37.9990%	34.4163%	27.8476%

Table 6.2. Percentage difference between measurement results and simulation results for different path loss index n_1, Scenario 2

	Rx1	**Rx2**	**Rx3**	**Rx4**	**Rx5**
n_2=4	36.7279%	41.6222%	55.6591%	50.3312%	31.2645%
n_2=5	36.6458%	41.4785%	55.6576%	50.2456%	31.2388%
n_2=6	36.9170%	41.8044%	55.6513%	50.3034%	31.2557%
n_2=7	36.6425%	41.4121%	55.6739%	50.2803%	31.2573%
n_2=8	36.7673%	41.6705%	55.6465%	50.2286%	31.2193%

Table 6.3. Percentage difference between measurement results and simulation results for different path loss index n_2, Scenario 1

	Rx1	**Rx2**	**Rx3**	**Rx4**	**Rx5**
n_2=4	16.9838%	26.9064%	44.1629%	40.2866%	33.4788%
n_2=5	13.0664%	22.8475%	40.2699%	36.3551%	29.6538%
n_2=6	9.1073%	18.8656%	36.4872%	32.9955%	26.3365%
n_2=7	5.6996%	15.3846%	32.8312%	29.3247%	22.7065%
n_2=8	2.7511%	12.3487%	29.2790%	26.0983%	19.6397%

Table 6.4. Percentage difference between measurement results and simulation results for different path loss index n_2, Scenario 2

Chapter 7

Proposition of a new model

In the aim to give the explanation of disparity between simulation results and measured data, a deeper analysis of model (5.1) is undertaken. At the first place, as already indicated, the model does not account for the reference path loss $PL(d_0)$. It does consider different path losses prior and after the break point, where the logarithm of first is taken with respect to reference distance d_0.

Revising the power law (2.7) and definition of path loss index given by Rappaport [2001]: *"the path loss exponent indicates the rate at which the path loss increases with distance"*, has given rise to idea that in propagation segment from wall up to the receivers a new path loss index should be valid. Signal level, significantly weaken by passing through the wall, should now decrease more rapidly then as before the wall. Also, signal paths from the barrier up to the receiving points will have different attenuations due to receivers' different distances from the barrier, as it may be observed in figure 5.4. If this new assumption is incorporated into model (5.1), and the reference path loss is added, the new model yields:

For case 1, $d < d_{bp}$:

$$PL(d) = PL(d_0) + n_1 10\log\left(\frac{d_{WALL}}{d_0}\right) + \frac{WAF}{\cos\theta} + n_2 10\log\left(\frac{d}{d_{WALL}}\right) \tag{7.1}$$

For case 2, $d > d_{bp}$:

$$PL(d) = PL(d_0) + n_1 10\log\left(\frac{d_{bp}}{d_0}\right) + n_3 10\log\left(\frac{d_{WALL}}{d_{bp}}\right) + \frac{WAF}{\cos\theta} + n_4 10\log\left(\frac{d}{d_{WALL}}\right) \tag{7.2}$$

The reference path loss $PL(d_0)$ is calculated according to (2.2):

$$PL(d_0) = -10\,log\left[\frac{G_t G_r \lambda^2}{(4\pi)^2 d_0^2}\right] = 10\,log\left[\frac{(4\pi)^2 d_0^2}{G_t G_r \lambda^2}\right] \tag{7.3}$$

For 2.4 GHz TelosB transceivers $\lambda = 0.125m$. The type of antenna embedded into TelosB platform is found in tel to be omni-directional Inverted-F antenna. Its gain can be looked up in inv. Hence, the transmitting and receiving antenna gains G_t and G_r will be equal and their value is 3.3 dB. Consequently, at reference distance d_0 of 1 m, the reference path loss is following:

$$PL(1m) = 10\,log\left[\frac{(4\pi)^2 \cdot 1^2}{3.3^2 \cdot 0.125^2}\right] = 29.676\,dB \tag{7.4}$$

WAF, $\cos\theta$ and d remain same as in (5.1). d_{WALL} is distance of the wall from the transmitter; this distance is obviously diverse for all five directions in two cases.

The new model assumes different path loss indexes, n_1, n_2, n_3 and n_4, for different propagation regions. In both equations (7.1) and (7.2), signal trajectories can be seen as divided in two segments separated by wall. In (7.1), n_1 is characterizing path loss from reference distance d_0 prior to the wall. When the signal passes through, it becomes attenuated for the factor of $WAF/\cos\theta$ and afterwards continues with free space propagation up to the receiver, which now has the new path loss index n_2. Situation is similar in (7.2), but as the break point occurs between d_0 and d_{WALL}, two regions will exist with distinctive path loss indexes n_1 and n_3, as detailed in Chapter 5 - Wall Attenuation Measurements. In the segment before the wall, signal level will additionally decrease due to the loss of Fresnel zone clearance. Thus, in the next segment after the wall, path loss will be again having the new path loss index n_4 (cannot be equal to n_2).

To the best of our knowledge, former is a fully new concept in empirical modeling of wireless signal propagation. Obtaining the values of n_1, n_2, n_3 and n_4 can be achieved by virtue of Linear Mean Square Error (LMSE) fitting.

Knowing the following parameters for wooden wall:

Wall Attenuation Factor WAF

Cosines of penetration angles for five receivers

Reference path loss $PL(d_0)$

Reference distance d_0

T-R separation distances d for both cases

The break point distance d_{bp}

Distance of the wall from the transmitter in five receiving directions d_{WALL}

a script was made in MATLAB which performs LMSE fitting of all four path loss indexes into measured data. The computation resulted in values below.

$$n_1 = 1$$

$$n_2 = 2$$

$$n_3 = 5.5$$

$$n_4 = 3$$

Former results are in agreement with possible theoretical values of path loss indexes for indoor environment, which may be found in Nikookar and Prasad [2009] and Feuerstein et al. [1994]. When they are plugged back into equations of the new model, (7.1) and (7.2), and simulated in MATLAB, significant improvement is achieved, as one might observe in figure 7.1.

The obtained values of path loss indexes may now serve the purpose for computation of brick wall attenuation factor WAF. Once again LMSE script was run in order to find the best fitting value, which turns out to be 9.9267 dB. With previous incorporated into the new model, results may be seen in figure 7.2. In Scenario 1, the measurements were possible for only three receivers due to the lack of space.

When styding figures 7.1 and 7.2 , it should be noted that parameters n_1, n_2, n_3, n_4 and brick WAF were fitted into measurements with high degree of dispersion. 'Simulation' curves might not be ideal in shape, however they tend to approach expected shape very closely.

Although the radio irregularity phenomena is incorporated in model, seems like the effects of reflection, diffraction and scattering made a large impact on signal propagation which resulted in uneven distribution of signal strength.

Percentage difference between the measurements and the results of new model simulation are shown in tables below.

	Rx1	**Rx2**	**Rx3**	**Rx4**	**Rx5**
Scenario 1	10.5404%	9.5880%	1.9635%	0.6468%	16.4983%
Scenario 2	15.2800%	10.8956%	3.1282%	3.4811%	2.0859%

Table 7.1. Percentage difference between measurement results and the results of new model simulation, wooden wall

	Rx1	**Rx2**	**Rx3**	**Rx4**	**Rx5**
Scenario 1	2.0085%	8.5978%	0.4615%		
Scenario 2	14.1677%	4.2248%	3.8750%	9.6487%	10.6550%

Table 7.2. Percentage difference between measurement results and the results of new model simulation, brick wall

For the wooden wall, percentage difference between measured and simulated results for all five receivers is reduced from 30.4915%, 35.2660%, 49.4429%, 44.1003% and 24.9983%, (which is the best result achieved with the old model for n_1=4 and n_2=4) to 10.5404%, 9.5880%, 1.9635%, 0.6468% and 16.4983% in Scenario 1. In Scenario 2, the smallest percentage difference between the old model simulation (n_1=3 and n_2=8) and the measured results is 2.7511%, 12.3487%, 29.2790%, 26.0983% and 19.6397%. With the new model, the values are 15.2800%, 10.8956%, 3.1282% , 3.4811% and 2.0859% for Scenario 2. One should note that different shapes of curves produced by the old and new model yield different results in percentage difference. As regard of brick wall, it can be concluded that percentage difference achieved with the new model is satisfactorily small.

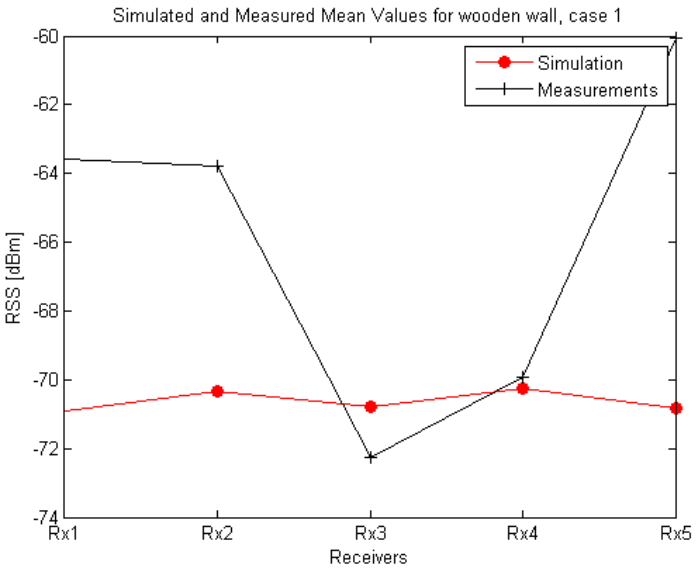

(a) Simulation results of the new model: wooden wall, Scenario 1

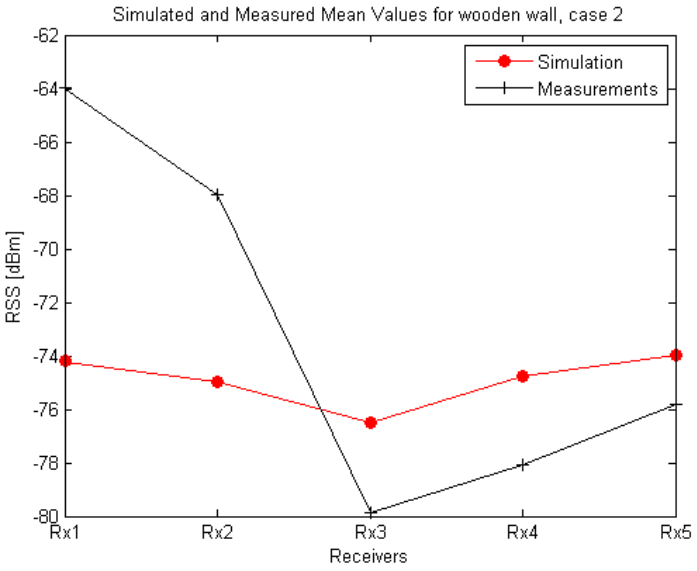

(b) Simulation results of the new model: wooden wall, Scenario 2

Figure 7.1. Simulation results of the new model for wooden wall

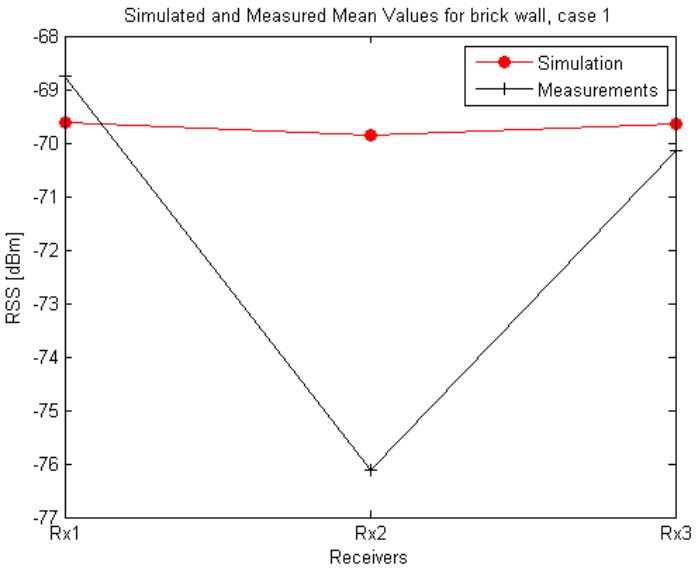

(a) Simulation results of the new model: brick wall, Scenario 1

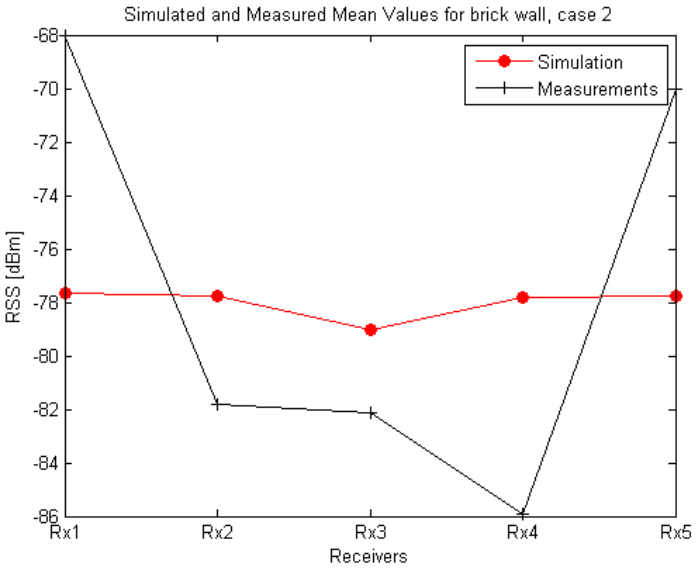

(b) Simulation results of the new model: brick wall, Scenario 2

Figure 7.2. Simulation results of the new model for brick wall

Chapter 8

Conclusion

In this work, exploration of empirical radio propagation model for indoor environment has been done. The 'Improved Empirical Model for Indoor Propagation Prediction' which incorporates the influences of Wall Attenuation Factor (WAF) and the break point distance into the path loss Power law, has been embedded into the Radio Irregularity Model with intent to increase the accuracy of prediction. Radio signal propagation through a single wall has been simulated in MATLAB and compared to the measurement results.

For the purpose of WAF analysis, measurements have been carried out for two types of walls - wooden wall and brick wall. The measurement results showed that the brick wall is introducing higher amount of attenuation with respect to wooden wall, which is in line with the expectations. Reflections, diffractions and scattering of the radio signal in furnished rooms have caused a significant dispersion of results.

Simulation has been performed in attempt to investigate whether the values of model's parameters found in research papers might be used directly in equations and thus make it possible to overcome the necessity of expensive and time-consuming measurements on-site. These parameters include WAF and the path loss indexes before and after the break point. In order to closely examine relation between WAF and the angle of penetration through the wall, one receiver has been placed from one side of the wall and five receivers from the other. Two scenarios have been established, one with the break point occurring before the wall and one without the break point. As it was not possible to obtain proper value of WAF for the brick wall, simulation has been done only for wooden wall. Enormous disparity has been found between the results of simulation and the measured values. It has been observed that convexities of simulation and measurement curves are opposite to one another. The difference between the measurements and simulation results for both scenarios ranges from 2.75% to 49.44%. As predicted by model, the angle at which the radio signal penetrates through the wall is proved to have influence on signal attenuation. However, it was observed the model does not account for reference path loss.

Based on the existing empirical model, a new better model has been originated by adding the reference path loss and introducing the new path loss index after the wall to account for different rates of signal loss from each side of the wall. The new path loss indexes have been

fitted into the measurement results by means of Linear Mean Square Error (LMSE). Simulation of the new model for wooden wall has showed significant improvement of propagation prediction. The average percentage difference between the measurements and the new simulation results is in range from 0.64% to 16.5% for both scenarios, which is almost three times less than the percentage difference achieved with the old empirical model. Using the new values of path loss indexes and employing LMSE it was possible to obtain WAF for the brick wall, which turned out to be higher than WAF for the wooden wall, as expected. Percentage difference between the measurements and simulation gained with the new model is satisfactorily small: 0.4615% - 14.1677%.

It was not possible to make use of values found in literature for parameters of the 'Improved Empirical Model for Indoor Propagation Prediction'. Not only the model itself fails in prediction, but also on-site measurements of the indoor environment in question must be performed in order to obtain necessary values for parameters.

As for the future work, performance of the new model might be explored for different types of walls, especially for those consisting of combined materials. Yet performing a small set of premeasurements makes it possible to simulate the environment without knowing too much about it, as already discussed. More interesting future work would be expansion of the new model for multiple walls and floors.

Glossary

DOI : Degree Of Irregularity

FAF : Floor Attenuation Factor

LMSE : Linear Mean Square Error

MAC : Medium Access Control

RIM : Radio Irregularity Model

RSS : Received Signal Strength

RSSI : Received Signal Strength Indicator

VSP : Variance of Sending Power

WAF : Wall Attenuation Factor

WSN : Wireless Sensor Networks

Bibliography

URL http://pdf1.alldatasheet.com/datasheet-pdf/view/125399/ETC1/CC2420.html.

URL http://www.ti.com/lit/an/swru120b/swru120b.pdf.

URL http://moss.csc.ncsu.edu/~mueller/rt/rt11/readings/projects/g4/datasheet.pdf.

a. URL http://en.wikipedia.org/wiki/Fresnel_zone.

b. URL http://en.wikipedia.org/wiki/Link_budget.

Les W. Barclay. *Propagation of Radiowaves, 2nd Edition*. The Institution of Engineering and Technology, 2002.

Christian Bettstetter and Christian Hartmann. Connectivity of wireless multihop networks in a shadow fading environment. *Wirel. Netw.*, 11(5):571–579, September 2005. ISSN 1022-0038. doi: 10.1007/s11276-005-3513-x. URL http://dx.doi.org/10.1007/s11276-005-3513-x.

Giuseppe De Marco, Tao Yang, Makoto Ikeda, and Leonard Barolli. Performance evaluation of wireless sensor networks for event-detection with shadowing-induced radio irregularities. *Mob. Inf. Syst.*, 3(3,4):251–266, December 2007. ISSN 1574-017X. URL http://dl.acm.org/citation.cfm?id=1376820.1376825.

M.J. Feuerstein, K.L. Blackard, T.S. Rappaport, S.Y. Seidel, and H. Xia. Path loss, delay spread, and outage models as functions of antenna height for microcellular system design. *Vehicular Technology, IEEE Transactions on*, 43(3):487–498, 1994. ISSN 0018-9545. doi: 10.1109/25.312809.

R. Hekmat and P. Van Mieghem. Connectivity in wireless ad-hoc networks with a log-normal radio model. *Mob. Netw. Appl.*, 11(3):351–360, June 2006. ISSN 1383-469X. doi: 10.1007/s11036-006-5188-7. URL http://dx.doi.org/10.1007/s11036-006-5188-7.

T. Muetze, P. Stuedi, F. Kuhn, and G. Alonso. Understanding radio irregularity in wireless networks. In *Sensor, Mesh and Ad Hoc Communications and Networks, 2008. SECON '08. 5th Annual IEEE Communications Society Conference on*, pages 82–90, 2008. doi: 10.1109/SAHCN.2008.20.

A. Muqaibel, A. Safaai-Jazi, A. Bayram, A. M. Attiya, and S.M. Riad. Ultrawideband through-the-wall propagation. *Microwaves, Antennas and Propagation, IEE Proceedings*, pages 581–588, 2005. ISSN 1350-2417. doi: doi:10.1049/ip-map:20050092.

R.D. Murch, J.H.-M. Sau, and K.W. Cheung. Improved empirical modeling for indoor propagation prediction. In *Vehicular Technology Conference, 1995 IEEE 45th*, volume 1, pages 439–443 vol.1, 1995. doi: 10.1109/VETEC.1995.504905.

H. Nikookar and R. Prasad. *Introduction to Ultra Wideband for Wireless Communications*. Signals and Communication Technology. Springer, 2009. ISBN 9781402066320. URL `http://books.google.rs/books?id=r-8TNQEACAAJ`.

Theodore S. Rappaport. *Wireless Communications : Principles and Practice*. Prentice Hall PTR, 2001.

S.Y. Seidel and T.S. Rappaport. 914 mhz path loss prediction models for indoor wireless communications in multifloored buildings. *Antennas and Propagation, IEEE Transactions on*, 40 (2):207–217, 1992. ISSN 0018-926X. doi: 10.1109/8.127405.

H. Xia, Henry L. Bertoni, L.R. Maciel, A. Lindsay-Stewart, and R. Rowe. Radio propagation characteristics for line-of-sight microcellular and personal communications. *Antennas and Propagation, IEEE Transactions on*, 41(10):1439–1447, 1993. ISSN 0018-926X. doi: 10.1109/8.247785.

Xiang Zeng, Rajive Bagrodia, and Mario Gerla. Glomosim: A library for parallel simulation of large-scale wireless networks. In *in Workshop on Parallel and Distributed Simulation*, pages 154–161, 1998.

Gang Zhou, Tian He, Sudha Krishnamurthy, and John A. Stankovic. Impact of radio irregularity on wireless sensor networks. In *in MobiSYS âĂŹ04: Proceedings of the 2nd international conference on Mobile systems, applications, and services*, pages 125–138. ACM Press, 2004.

Gang Zhou, Tian He, Sudha Krishnamurthy, and John A. Stankovic. Models and solutions for radio irregularity in wireless sensor networks. *ACM Trans. Sen. Netw.*, 2(2):221–262, May 2006. ISSN 1550-4859. doi: 10.1145/1149283.1149287. URL `http://doi.acm.org/10.1145/1149283.1149287`.